Vol. 727: 67–80, 2024
https://doi.org/10.3354/meps14489

MARINE ECOLOGY PROGRESS SERIES
Mar Ecol Prog Ser

Published January 25

Phytoplankton community changes in relation to nutrient fluxes along a quasi-stationary front

Jørgen Bendtsen[1,*], Niels Daugbjerg[2], Rune Stefan Jensen[2], Mariska Catherine Brady[3], Morten Holtegaard Nielsen[4], Jørgen L. S. Hansen[5], Katherine Richardson[3]

[1]Globe Institute, Section for Geobiology, University of Copenhagen, Øster Voldgade 5–7, 1350 Copenhagen K, Denmark
[2]Marine Biological Section, Department of Biology, University of Copenhagen, Universitetsparken 4, 2100 Copenhagen Ø, Denmark
[3]Globe Institute, Section for Biodiversity, University of Copenhagen, Universitetsparken 15, 2100 Copenhagen Ø, Denmark
[4]Marine Science & Consulting, Peder Lykkes Vej 8, 4 th., 2300 Copenhagen S, Denmark
[5]Department of Ecoscience, Aarhus University, Frederiksborgvej 399, 4000 Roskilde, Denmark

ABSTRACT: The main strait (Great Belt) connecting the North Sea and the Baltic Sea constitutes a quasi-stationary front and exposes phytoplankton to various degrees of water column mixing. Here, we examine phytoplankton community distributions (using the cell abundance of 4 readily identifiable diatoms) and estimate new production along the strait during early spring. Vertical turbulent mixing was ~10 times greater at stations in the strait compared to stations outside the strait. New production in the strait was on average ~50 mg C m^{-2} d^{-1}, i.e. 8% of the average total primary production, and could explain the increase in chlorophyll observed along the strait. A non-metric multidimensional scaling analysis of phytoplankton community composition showed significant spatial groupings. However, variation of species abundances could not be explained by the general transport, where the abundance of the largest species decreased during the passage of the strait. A relatively small species (*Guinardia delicatula*) showed an increasing dominance in and above the subsurface chlorophyll maximum along the strait, and the bottom layer was also correspondingly dominated by a relatively small species (*Skeletonema marinoi*). This phytoplankton composition could be explained by photosynthetic traits associated with more efficient light usage of small cells together with increased nutrient supply in the strait.

KEY WORDS: New production · Diatoms · Phytoplankton community · Phytoplankton traits · Turbulent nutrient fluxes · Primary production · Great Belt

1. INTRODUCTION

Changes in nutrient and light availability caused by vertical water column mixing can potentially influence primary production and phytoplankton composition. Directly observing how mixing influences these processes is, however, seldom possible under *in situ* conditions. The Great Belt, one of 3 narrow straits connecting the Baltic Sea and the North Sea, provides a unique and bounded system in which to observe phytoplankton responses to mixing. Through the 3 straits joining these 2 seas, the surplus freshwater from runoff exits the Baltic Sea. Intrusions of high-saline water enter the straits from the north and maintain the salinity balance in the Baltic. The large-scale density differences across the straits establish an estuarine layered flow with low-saline out-flowing surface water and high-saline in-flowing bottom water from the North Sea. In addition, significant barotropic exchange (i.e. a uniform displacement of the entire water column) is driven by sea-level differences across the strait induced by wind-forcing from passing atmospheric low-pressure systems and may cause large inflow of bottom water to the Baltic (e.g.

*Corresponding author: jorgen.bendtsen@sund.ku.dk

Publisher: Inter-Research · www.int-res.com

Lehmann et al. 2022). Most water to the Baltic is transported through the central strait via the Great Belt (Jakobsen & Trébuchet 2000, Stanev et al. 2018), where the topographic constriction and the relatively shallow depths establish a quasi-stationary frontal system between the 2 water masses of Baltic and North Sea (Atlantic) origin.

Mixing between surface and bottom water masses is more intense in the strait than in the neighboring areas (Bendtsen et al. 2009). This mixing has a major influence on oxygen (Hansen & Bendtsen 2013) and nutrient conditions (Reissmann et al. 2011) in the inflow to the western Baltic Sea. Analysis of long time series shows that surface water is enriched by nutrients from the bottom water in the strait (Hansen & Mohn 2021); thus, mixing in the strait has a regional as well as a local biogeochemical impact.

Primary production is elevated in the strait compared with ambient waters in the Kattegat and the Baltic (Rydberg et al. 2006, Lund-Hansen et al. 2008, Lyngsgaard et al. 2014), and decadal time series of phytoplankton biomass show higher values in the strait than in the western Baltic Sea located south of the strait (based on cell counts; Henriksen 2009). Phytoplankton composition generally differs between the Baltic and the Belt Sea area, e.g. cyanobacteria are always present in the western Baltic whereas diatoms tend to dominate in the strait (Henriksen 2009). Spatial gradients in phytoplankton community composition also characterize the area from the Baltic proper to the western Baltic Sea (Wasmund et al. 2011). In addition, microbial communities show large-scale gradients from the northern Baltic Sea through the Great Belt and into the North Sea (Herlemann et al. 2011).

The purpose of this study was to quantify the role of vertical nutrient fluxes on biological production and phytoplankton community composition. First, we analyzed variations in nutrients and chlorophyll distributions and related these to vertical mixing and estimates of new and primary production in and around the Great Belt. We then examined the distributions of 4 dominating diatom species in relation to the circulation in the strait. Finally, we analyzed their variation in relation to traits of light adaptation in the strait.

2. MATERIALS AND METHODS

2.1. Overview

The Great Belt area was investigated from RV 'Aurora' (Aarhus University, Denmark) in the period 25–29 March 2019, when mixing, nutrients and the abundances of 4 dominating diatom species were determined along the strait (Fig. 1a). The strait is ~100 km long and relatively narrow (typically ~25 km wide with a minimum of ~10 km in the southern part). The depth in the Great Belt varies between 20 and 60 m, with the variation being due to the presence of several small deep basins and shallow plateaus. The northern end station of the transect was located outside the strait in the southern Kattegat, while the southernmost station of the transect was located in the western Baltic Sea. Stations were located along the deepest part of the strait and covered relatively deep areas (>50 m), areas with large bottom curvature and narrow constrictions. The northern- and southernmost stations are referred to as end-member stations in the water mass analysis.

Water sampling, vertical profiling of water properties, and turbulence measurements were carried out during daytime (06:00–20:00 h UTC). Estimates of turbulent fluxes were made for 2 sections of the transect separated at 55.5° N, i.e. approximately in the middle of the strait, and referred to as the northern and southern sectors, respectively (Fig. S1 in the Supplement at www.int-res.com/articles/suppl/m727p067_supp.pdf). The density gradient in the surface layer motivated this division of the strait into 2 sectors. A high-resolution bathymetric atlas was applied to create Fig. 1 (GEBCO Bathymetric Compilation Group 2020, 15 arc-second resolution, i.e. <450 m). Note, however, that this horizontal resolution does not resolve the narrow deep channels in the seabed. Data analyses applied R (R Core Team 2021) for linear regression and analysis of similarities (ANOSIM) and the R-based BSDA-package of Welch modified 2-sample *t*-test (Arnholt & Evans 2021) for the statistical analysis of vertically integrated chlorophyll *a* (chl *a*), estimated primary (PP) and new production (NP) between different sections of the strait (Kolmogorov-Smirnov tests were applied for testing normality, i.e. $p > 0.05$, of the distributions).

2.2. Vertical profiles and water sampling

Conductivity, temperature and pressure (depth) were measured with a Seabird 911+ system (CTD), and water samples were collected by 12 rosette-mounted 5 l Niskin GO-bottles. Salinity is reported as absolute salinity (S_A; IOC et al. 2010). Chl *a* fluorescence (Wet Labs ECO-AFL/FL fluorometer) and photosynthetically available radiation (PAR; Licor sensor) were measured along with CTD-profiles at 17 stations (Fig. 1a).

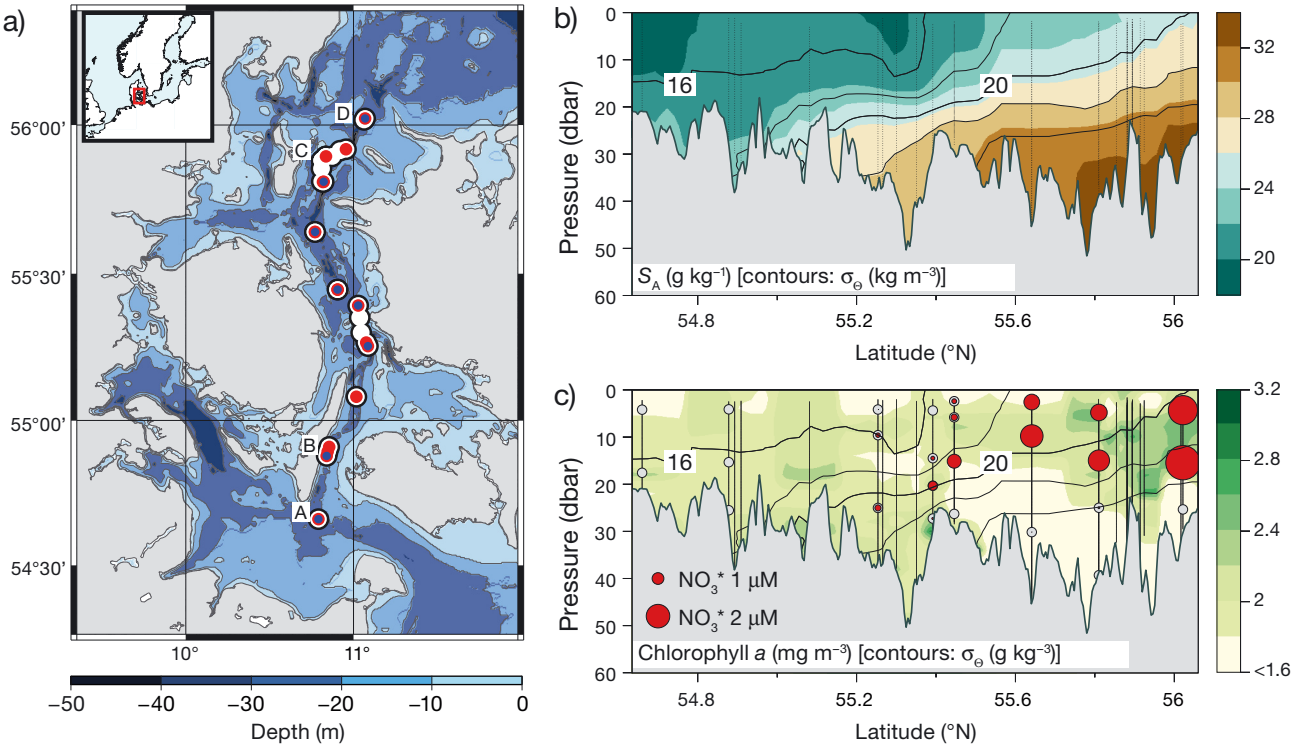

Fig. 1. (a) Stations in the Great Belt with measured turbulence profiles (white circles), conductivity, temperature, depth (CTD) profiles (red bullets) and water sampling for nutrients determinations (blue bullets). Inset shows the location of the study area (red square) in the North Sea-Baltic Sea transition zone. Stations shown in Fig. S2 are indicated by letters (A–D). (b) Vertical transect of absolute salinity (S_A) (colors, g kg^{-1}) in the strait. Contour lines show potential density anomalies (σ_Θ in intervals of 2 kg m^{-3}). (c) Section of chlorophyll (colors, mg m^{-3}) in the strait where locations of nitrate samples are indicated with gray or red bullets (contour lines show σ_Θ). Estimated nitrate uptake (NO_3^*, mmol N m^{-3}) is shown with red circles (proportional to the radius)

Velocity profiles from an acoustic doppler current profiler (ADCP; RDI Sentinel Workhorse 600 kHz) mounted on an undulating ScanFish (5 knots) were averaged in 5 min intervals from 10 passages of a central location in the Strait (55.5° N, 10.91° E) during the period 26–29 March 2019.

2.3. Turbulence measurements

Profiles of turbulence were made with a freely sinking Rockland Scientific International (RSI) VMP-250 microstructure vertical profiler (sinking speeds ~0.7 m s^{-1}) equipped with 2 shear probes, an additional CTD (JFE Advantech, JAC), and a CLTU-VMP-250 sensor for measurements of fluorescence. Microstructure measurements of shear and fluorescence were sampled at 64 Hz. The instrument was calibrated before the cruise. In total, turbulence profiles were made at 30 stations (7 stations were visited twice; Fig. 1a) and, typically, 3–5 casts were made at each station (in total 142 casts, Table S1).

2.4. Nutrients and chl *a*

Water samples were collected from the surface (~5 m), mid-depth (~15 m), and from the bottom water (>20 m). Water was pre-filtered (0.2 µm) and stored at −20°C on the ship and −80°C in the land-based laboratory. Nutrient concentrations (nitrite, nitrate, ammonia, phosphorus, and silica) and total nitrogen (TN) were analyzed by wet-chemistry methods according to Grasshoff et al. (1983) at Aarhus University; detection limits were: 0.04 (NO_2^-), 0.1 (NO_3^-), 0.3 (NH_4^+), 0.06 (PO_4^{3-}) and 0.2 (Si) and 1.0 µM (TN), respectively.

A derived value for the nitrate deficit (NO_3^*) was defined as: $NO_3^* = NO_3(S_A) - NO_3(obs)$. The nitrate deficit expresses the difference between the expected nitrate concentration that would result from mixing between 2 end-members, i.e. $NO_3(S_A)$ observed at the salinity S_A, and the actual value, $NO_3(obs)$. Thus, a positive value of NO_3^* indicates that internal sinks, e.g. biological consumption, have consumed nitrate. The relationship between nitrate and salinity, i.e.

NO_3(S_A), was determined from observations along the strait.

Chl *a* (captured on GF/F filters; referred to as chlorophyll below) was measured with a calibrated standard (DHI Lab) on a Trilogy Laboratory fluorometer (Turner Designs). The fluorometers on the vertical microstructure turbulence (VMP)-profiler and the rosette (CTD) showed general agreement with each other (i.e. linear regression resulted in $R^2 = 0.61$, n = 61, $p < 0.001$), whereas there were no significant linear correlations between the instruments and the chlorophyll measurements from the water samples. This could be explained by a generally weak vertical gradient of chlorophyll in the area (chlorophyll ranged between 1.5 and 3.5 mg chl m^{-3}, except for 2 samples at ~0.5 and 1 mg chl m^{-3} sample at 4 mg chl m^{-3}). Therefore, the calibration was based on a linear regression with a forced zero-intercept between chlorophyll (chl) and fluorescence (fl). This resulted in a high correlation between both the VMP fluorescence (chl = 0.86 fl, $R^2 = 0.93$) and the CTD-fluorescence (chl = 0.79 fl, $R^2 = 0.93$). Vertically integrated chlorophyll, estimates of biomass and PP were based on the linear regressions.

2.5. Distribution of dominant diatoms

Water collected in Niskin bottles was filtered through a 500 µm net (to remove zooplankton), and samples were left to settle in 50 ml sedimentation cylinders (Hydrobios setup) for at least 24 h (Helcom 2021). Cell counts were made on samples fixed in Lugol's iodine solution (2% final concentration) (Utermöhl 1958) using an inverted Nikon light microscope (Eclipse Ts2R). Four easily identifiable and abundant centric diatom species were assessed: *Guinardia delicatula*, *Proboscia alata*, *Rhizosolenia setigera* and *Skeletonema marinoi*. At least 400 units (chains or single individuals) of the most abundant species, *G. delicatula*, were counted while the entire chamber was counted for the other species. Water samples from 7 stations were enumerated from 3 depth levels (5, 15, and 25 m). The relative contribution of the 4 species to the total phytoplankton biomass (estimated from observed chl *a* and an estimated C:chl ratio) was estimated from representative carbon to cell ratios of the 4 species. Spatial distributions of different communities defined from the 4 species were identified from a non-metric multidimensional scaling (NMDS) analysis. The analysis was made in R using the vegan package (Oksanen et al. 2020).

2.6. Calculating turbulent diffusivity

The dissipation rate of turbulent kinetic energy (ε) was calculated from the velocity shear with software provided by Rockland Scientific (ODAS, ver. 4.0; Douglas & Lueck 2015). Values of ε were estimated from depths below 5 m to reduce possible disturbances from the ship (with a draught of 2.75 m). These were analyzed in bins of 8 s with 50% overlap, corresponding to a resolution of ~5 m (Wolk et al. 2002, Lueck 2016). Each cast provided 2 shear measurements, and there was generally relatively small deviation between the ε estimates from the 2 shear sensors. Outliers due to noise introduced during the operational procedure were identified by first inspecting the profiles visually for spikes (2 profiles were removed). Finally, a quality criterion of acceptable difference between the 2 shear sensors was defined (Bendtsen & Richardson 2018) by analyzing the error distribution of all data below 10 m depth, defined as the difference of the logarithm ($\log_{10}$) between the ε estimates (W kg^{-1}) from the 2 shear probes. The error distribution had an absolute SD of 0.14 (n = 1467). For measurements to be included in the analysis, the difference between the 2 sensors on the same profile should be less than 3 times the absolute deviation. This led to the removal of less than 6% of the pairs of ε from the data set.

The vertical turbulent diffusion coefficient was calculated from the ratio of ε and stratification, i.e. the tendency of turbulent motion to break the local stability in the water column. Stratification is expressed by the Brunt-Väisälä frequency (N^2) and is calculated from the slope of a linear regression of density measurements in 4 m segments. The vertical diffusion coefficient is calculated as $K_v = \Gamma\varepsilon/N^2$ (Osborn 1980), where Γ is the mixing efficiency and is parameterized from a relationship between the mixing efficiency and the buoyancy Reynolds number (Bouffard & Boegman 2013).

2.7. Vertical turbulent fluxes

Vertical turbulent fluxes of salinity and nitrate F_Φ, with Φ representing salinity (S) or nitrate (N), were calculated from the vertical tracer gradient (Φ_z) and the vertical turbulent diffusion coefficient (K_v):

$$F_\Phi = -K_v\Phi_z \quad (1)$$

The vertical salinity gradient was calculated from linear regression of a 2 m segment of salinity measurements from the JAC-CTD and the salinity flux (F_S)

was calculated from Eq. (1). The vertical spacing between nutrient samples was relatively large and, therefore, nitrate fluxes (F_N) were calculated by transforming the nitrate flux in relation to the salinity gradient and F_S:

$$F_N = -K_v \frac{\partial N}{\partial z} = -K_v \frac{\partial N}{\partial S}\frac{\partial S}{\partial z} = \frac{\partial N}{\partial S} F_S \qquad (2)$$

The vertical nitrate (N) gradient (z is the vertical coordinate) with respect to salinity (S) was determined from the slope of a linear regression of nitrate samples versus absolute salinity. Nitrate concentrations at some stations were not well represented by a simple mixing line and this caused an under-estimation of F_N calculated by Eq. (2). This limitation was considered in the analysis.

2.8. Estimating primary production

PP was estimated from satellite derived surface PAR, profiles of chlorophyll and PAR, and climatological values of photosynthetic parameters from the area. Satellite measurements of PAR from MODIS Aqua level-3 (Frouin et al. 2012) (9.3 km resolution) from the period 22–30 March 2019 were averaged in the area (10.5–11.5° E, 54.5–56.1° N), and the resulting daily averaged surface PAR of 23.54 E m^{-2} d^{-1} was used as representative for the incoming light during the cruise. PAR during the day was calculated from the hourly clear sky insolation for a location in the middle of the strait (11° E, 55.5° N, 28 March), and the total insolation during the day was then scaled to equal the satellite derived daily PAR.

Vertical distributions of chlorophyll were determined from the chlorophyll-calibrated fluorometer from the turbulence-profiler (sampled at 64 Hz) and averaged in bins of 0.1 m. The vertical distribution of PAR was assumed to follow Beer's law (i.e. PAR(z) = PAR($z = 0$) exp(k_{att} z), $z \leqslant 0$) and the light attenuation (k_{att}) was calculated from linear regression of the logarithm of PAR versus depth in the upper 20 m at each station. The average k_{att} from all CTD stations (made during daylight, n = 13) was 0.23 ± 0.02 m^{-1} (mean ± SE), and the bottom depth of the euphotic zone (d_{eup}, i.e. the 0.1% PAR level) was 29.9 ± 2.8 m. Thus, the major part of the water column was within the euphotic zone in the relatively shallow strait.

Lyngsgaard et al. (2014) analyzed the seasonal variation of photosynthetic parameters in the Baltic Sea transition zone, including the Great Belt, based on 1385 water column photosynthesis estimates in the period 1998–2012, and typically ~50 annual estimates were made at the surface and in the subsurface chlorophyll maximum (SCM) in the strait. The difference between values at the surface and the SCM was relatively small during early spring, and representative values in March for the entire water column (i.e. average values of surface and SCM values) of the maximum photosynthetic rate (P^B_{max}) and the photosynthetic response at low light levels (α^B) were estimated to 2.15 ± 0.63 g C (g chl)$^{-1}$ h^{-1} and 0.037 ± 0.006 µg C (µg chl h µE m^{-2} s^{-1})$^{-1}$, respectively. The error-estimates corresponded to a variation of ±29 and ±18% of P^B_{max} and α^B, respectively. Thus, we estimate that the values of the photosynthetic parameters derived from the climatological values implied an uncertainty of ~30% on the PP estimates.

PP was calculated from vertical profiles of chlorophyll, light and photosynthetic parameters (Webb et al. 1974, Bendtsen & Richardson 2018) and vertically integrated (z) from the bottom of the euphotic zone and during a 24 h period (t):

$$PP = \int_0^{24h}\int_{-d_{eup}}^{0} P^B_{max}\,chl(z)\left\{1-\exp\left[-PAR(t,z)\frac{\alpha^B}{P^B_{max}}\right]\right\}dz\,dt \qquad (3)$$

2.9. Estimating new production

NP is defined as the magnitude of PP that can be supported by nitrate being transported into the euphotic layer (Dugdale & Goering 1967). We estimate NP from the nitrate flux by assuming a constant C:N molar ratio of $\gamma_{C:N}$ = 106/16 (Redfield et al. 1963) and that all nitrate in the surface layer is consumed by phytoplankton, in accordance with the low nitrate concentrations observed in this layer. The nitrate flux into the euphotic zone was calculated from its maximum value, i.e. F_N(max), in the depth range between 15 and 29.9 m (i.e. the lower part of the euphotic zone), and NP (converted to carbon mass by m_C) is then estimated from NP = m_C $\gamma_{C:N}$ F_N(max).

3. RESULTS

3.1. Overview

The entire strait constituted a frontal zone between surface water from the Baltic Sea and bottom water originating in the North Sea (Fig. 1). In general, there was a relatively small temperature difference between the surface (~6°C) and the slightly colder bottom water (~5.5°C), reflecting the typical situation in the area in early spring. The lowest salinity (S_A =

18.90 g kg^{-1}) was observed in the surface water at the southernmost station in the western Baltic and the highest salinity (S_A = 33.16 g kg^{-1}) was found in the bottom water at the northernmost station in the Kattegat (Fig. 1b). The highest chlorophyll concentrations were observed in the northern part of the Great Belt (Fig. 1c).

3.2. Nutrient distributions

The strait was characterized by nutrient-poor surface water (originating from the Baltic) and nutrient-rich bottom water (originating from the North Sea) (Fig. 2a). The distribution of nitrate versus S_A indicated that nitrate concentrations in the majority of the samples could be explained by mixing between waters found at the 2 end-member stations where the southern and northern end-members represent surface and bottom water properties, respectively. Surface samples with a relatively high salinity (S_A > 24) did not, however, fit this pattern as nitrate concentrations here differed significantly from a mixing line (i.e. a line between 2 end-member properties) between these 2 end-members (Fig. 2a, orange triangles). This deviation indicated an internal nitrate sink, presumably resulting from biological activity. A mixing line between surface and bottom water was identified by excluding these samples from the surface layer data: $NO_3(S_A) = -7.8 + 0.38\ S_A$ (R^2 = 0.96, $p < 0.001$) implying an end-member nitrate concentration at the southern (northern) end of the strait with S_A=19 g kg^{-1} (31 g kg^{-1}) of 0.26 mmol N m^{-3} (4.9 mmol N m^{-3}).

Ammonia (0.25–1.72 mmol m^{-3}) exhibited no significant variation in relation to salinity (not shown). Nitrite concentrations were relatively low (0–0.29 mmol m^{-3}) along the entire strait. Total dissolved nitrogen (0.2 µm filtered) varied between 12 and 30 mmol m^{-3} and did not correlate strongly with salinity (R^2 = 0.29). We note that mixing and subsequent remineralisation of dissolved organic matter may be an additional source of nutrients in the euphotic zone (Hansen & Bendtsen 2014). However, there were no significant vertical gradients in TN (not shown), suggesting that the role of organic matter as an internal nitrogen source was relatively small. Thus, nitrogen input along the strait was mainly due to vertical mixing of nitrate.

Silicate also demonstrated a significant linear regression to salinity (Fig. 2b; R^2 = 0.93, $p < 0.001$). The high-saline and nitrate-depleted surface water samples also contained lower silicate concentrations than would have been expected from mixing between the 2 end-members (Fig. 2b, orange triangles). Similarly, phosphate exhibited a gradient between surface and bottom waters and a significant linear regression in relation to salinity (Fig. 2c; R^2 = 0.8, $p < 0.001$). The relatively high-saline surface water samples (orange triangles) were also characterized by low phosphate concentrations (<0.1 mmol m^{-3}), similar to the nitrate distribution. Relatively high phosphate concentrations were seen in surface samples in the southern part of the strait (PO_4^{3-} > 0.2 mmol m^{-3} and S_A < 21 g kg^{-1}) and indicated a local source. However, this source could not be identified from our data set and was not analyzed further.

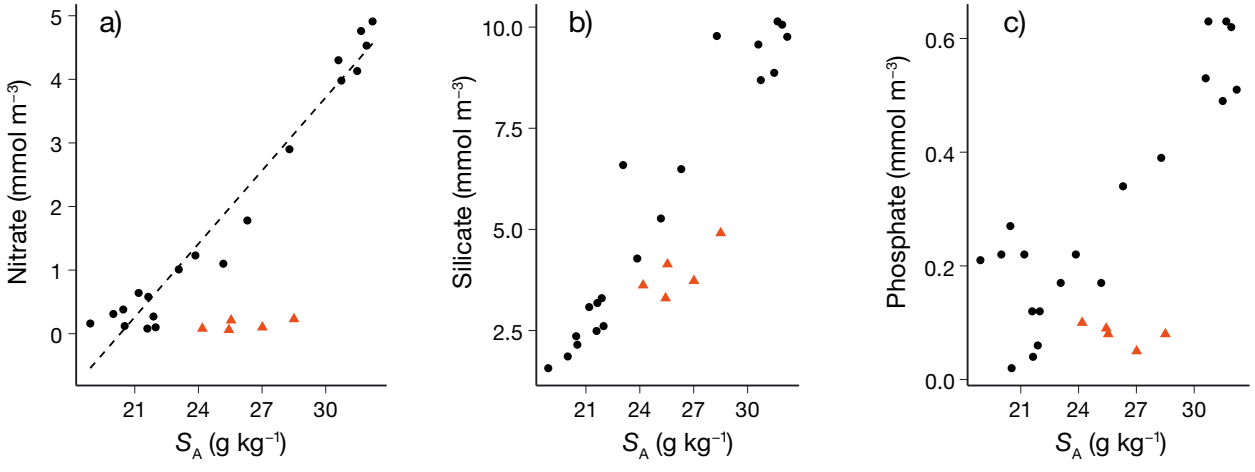

Fig. 2. (a) Nitrate, (b) silicate and (c) phosphate concentrations versus absolute salinity (S_A). Surface water samples influenced by mixing with high-saline bottom water are shown with orange triangles and the remaining water samples as black circles. Dashed line in (a) shows linear regression of the remaining water samples

3.3. PP and gradients in the surface layer

Horizontal gradients in the surface waters of the Great Belt were identified by integrating the upper 20 m of salinity and chlorophyll (integrating to the bottom of the euphotic zone, i.e. 29.9 m, would include stations with more shallow bottom depths). PP was integrated for the euphotic zone (2 shallow profiles with depth less than 25 m were omitted). Average values were calculated for all casts at each of the 2 end-member stations and in the 2 sectors (Table 1).

Salinity in the upper 20 m (Fig. 3a, Table 1) showed a gradual northward increase and chlorophyll showed a similar increase from 45 to 53 mg chl m^{-2}, although with more scatter at each station (Fig. 3b, Table 1). The average estimated PP in the entire strait was 0.59 ± 0.06 g C m^{-2} d^{-1} (n = 139). The northward increase in chlorophyll was also reflected in the distribution of PP, where PP increased from 0.50 to 0.65 g C m^{-2} d^{-1} from the southern to the northern end-member station (Fig. 3c, Table 1). PP estimates for the northern sector were also significantly ($p < 10^{-4}$, df = 122.3, t = −9.78) higher than for the southern sector.

3.4. Nitrate deficit in high-saline surface water

Nitrate concentrations were generally distributed along a mixing line between 2 end-members representing surface water at the southernmost station and bottom water at the northernmost station, i.e. $NO_3(S_A)$ shown as a dashed line in Fig. 2a. However, a clear deviation was seen for high-saline surface water, implying a relatively large nitrate deficit ($NO_3^\star$). The distribution of $NO_3^\star$ showed a gradual increase in the surface layer from about the middle of the strait going northwards, and the largest deviations were seen at the northernmost station (maximum $NO_3^\star$ = 2.9 mmol m^{-3}), where the highest concentrations of chlorophyll also were observed (Fig. 1c).

Table 1. Average values (SD, no. of data) in the upper 20 m of absolute salinity (S_A) and chl *a*, and vertically integrated primary production (PP), and new production (NP) in the euphotic zone at the southern and northern end-member stations (S-endm and N-endm, respectively) and the southern and northern sectors

Area	Latitude (°N)	n	S_A (0–20 m) (g kg^{-1})	Chl *a* (0–20 m) (mg m^{-2})	PP (g C m^{-2} d^{-1})	NP (g C m^{-2} d^{-1})
S-endm	54.66	5	19.44 ± 0.05	44.90 ± 0.64	0.50 ± 0.01	0.008 ± 0.003
Southern sector	54.66–55.22	48	21.13 ± 1.03	46.70 ± 1.79	0.55 ± 0.03	0.070 ± 0.059
Northern sector	55.85–56.02	77	25.88 ± 0.74	53.16 ± 3.53	0.62 ± 0.05	0.038 ± 0.041
N-endm	56.02	9	27.60 ± 0.13	53.15 ± 1.11	0.65 ± 0.02	0.006 ± 0.003

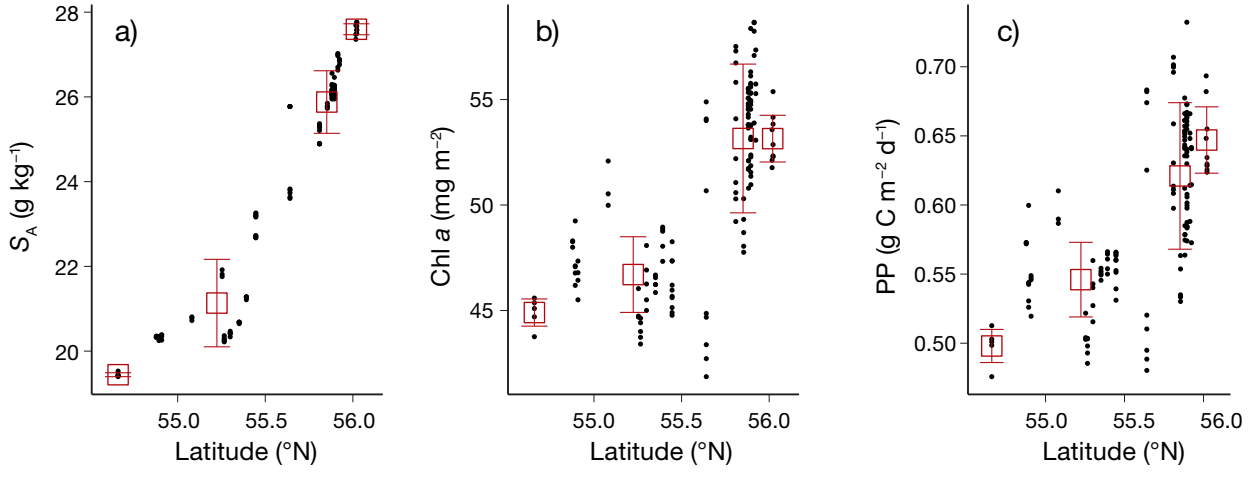

Fig. 3. (a) Average values of absolute salinity (S_A), (b) chlorophyll in the upper 20 m, and (c) primary production (PP) in the euphotic zone. Average values and SD of values at the end-member stations and for the 2 sectors are shown with red squares (SD, see also Table 1)

3.5. Vertical profiles and salinity fluxes

Distributions along the Great Belt at 4 stations showed the gradual influence from vertical mixing on properties in the surface and bottom layers (Fig. S2). A relatively sharp halocline between 15 and 20 m depth separated the bottom and surface layers at the southern end-member station and the strong stratification resulted in a salinity flux (F_S) close to zero (Fig. S2e). Mixing in the southern sector of the strait could explain the almost homogeneous chlorophyll distribution in the upper 30 m and the weak halocline between 10 and 30 m (Fig. S2b,f). The resultant maximum salinity flux was 0.07 g m^{-2} s^{-1} at the bottom of the euphotic zone.

Salinity in the northern sector (Fig. S2c,g) was significantly higher, with turbulent diffusion coefficients at mid-depth of ~10^{-4} m^2 s^{-1} and a corresponding salinity flux of 0.05 g m^{-2} s^{-1}. A relatively strong halocline at the northern end-member station at between 18 and 22 m depth separated the high-saline bottom water from the surface layer. This layered structure was mirrored in the chlorophyll profile where a weak SCM and low vertical mixing across the pycnocline ($K_v < 10^{-6}$ m^2 s^{-1}) resulted in a relatively small salinity flux.

3.6. Turbulent mixing along the strait

Mixing parameters were binned and averaged in 5 m intervals from 5 m to the bottom (Fig. 4a–c). In general, ε was relatively low at the end-member stations (~5×10^{-8} W kg^{-1}) except near the surface and

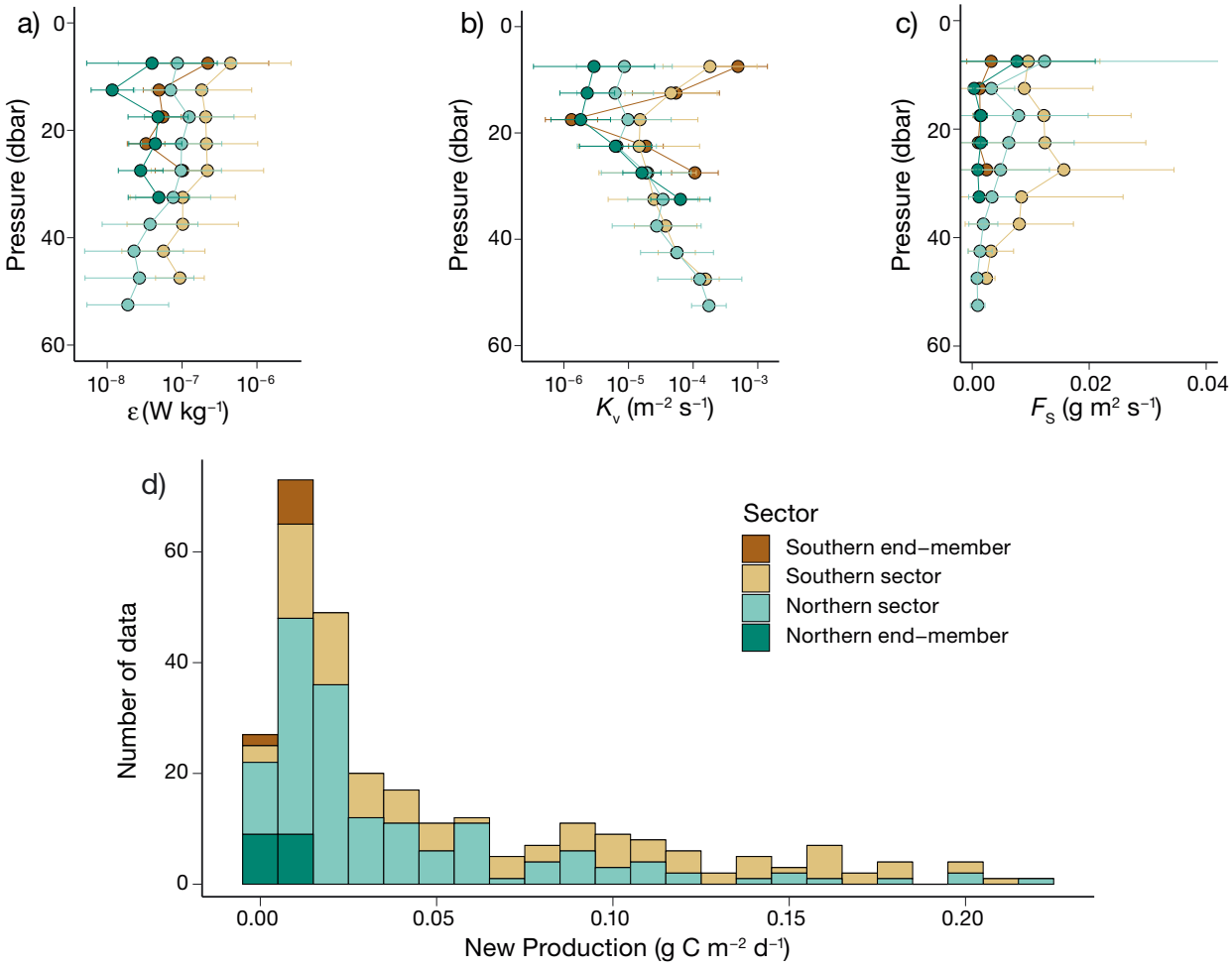

Fig. 4. (a) Average values of the dissipation rate of turbulent kinetic energy (ε), (b) the vertical turbulent diffusion coefficient (K_v), and (c) the turbulent diffusive vertical salinity flux (F_S). Values are averaged at the 2 end-member stations and in the 2 sectors and show the (a,b) geometric mean and standard factor and the (c) average and standard deviation. (d) Frequency distribution of estimates of new production (NP) from all casts and divided into the 2 end-member stations and the 2 sectors

close to the bottom. The largest average values at mid-depth (15–25 m) were seen in the southern sector (~2×10^{-7} W kg^{-1}) and with slightly lower values of ε in the northern sector (~1×10^{-7} W kg^{-1}).

Surface values of K_v at the southern end-member station were also relatively large because of a vertically homogeneous surface layer and weak stratification ($N^2 < 10^{-5}$ s^{-2}). The well-defined 2-layer structure also resulted in a strong stratification in the pycnocline ($N^2 \sim 10^{-2}$ s^{-2}). This explains the low K_v between 15 and 20 m depth at this station ($K_v \sim 10^{-6}$ m^2 s^{-1}). K_v values at the northernmost station were also relatively low (~10^{-5} m^2 s^{-1}) except for an increase towards the bottom (K_v ~6×10^{-5} m^2 s^{-1} below 30 m depth). Mid-depth values in the northern and southern sectors ranged between 0.6 and 1.5×10^{-5} m^2 s^{-1} and increased to ~10^{-4} m^2 s^{-1} at 50 m depth.

3.7. New production

The average NP of all casts along the transect was 50 ± 50 mg C m^{-2} d^{-1}, corresponding to about 8% of the average PP. The average depth of the maximum vertical nitrate flux was 21.7 ± 4.4 m among all casts. This depth level corresponded to the isopycnal of 18 kg m^{-3} in the northern sector and was approximately at the same depth level as the shallow plateaus in the southern sector. The relatively large standard deviation in the average NP reflected a large spatial variation along the strait (Table 1). The 2 end-member stations, north and south of the strait, respectively, were characterized by low NP (< 0.020 g C m^{-2} d^{-1}), whereas relatively large NP values characterized the southern and northern sectors with maximum values of up to 220 mg C m^{-2} d^{-1} and mean values of 70 (n = 100) and 38 mg C m^{-2} d^{-1} (n = 156), respectively. The NP distributions in the 2 sectors (Fig. 4d) were skewed towards low values and, in general, with more high values in the southern sector. The difference between the mean values in the 2 sectors was significant ($p < 10^{-4}$, df = 169.1, t = 4.57).

3.8. Distribution of four diatom species

The greatest surface and mid-depth concentrations of *Proboscia alata* and *Rhizosolenia setigera* were seen in the southern part of the strait (i.e. 5000–15 000 and ~400 cells l^{-1}, respectively) whereas only low concentrations (< 250 and ~0 cells l^{-1}, respectively) were observed in the northern sector (Fig. 5). Similar gradients in the abundances of these species were seen in samples from the bottom layer, although *R. setigera* was also observed in low concentrations at the northernmost station. The opposite tendency was seen for *Guinardia delicatula*, for which high mid-depth concentrations (> 600 000 cells l^{-1}) were observed at the northern station. These decreased gradually to values below 150 000 cells l^{-1} in the southern part of the strait and towards the southern end-member station. Similar gradients were observed in samples from the surface and the bottom layers. Bottom water concentrations of *Skeletonema marinoi* (5000–20 000 cells l^{-1}) were significantly greater than at the surface and mid-depth (< 2800 cells l^{-1}).

The contribution of the 4 species to the total phytoplankton carbon (C) biomass was calculated from the cell abundance and the estimated C-content of the 4 species and then compared with the biomass estimated from the vertically integrated chlorophyll calculated from fluorescence profiles, i.e. ranging between 1.7 and 2.1 gC m^{-2} with a C:chl of ~40 g g^{-1} (Jakobsen & Markager 2016) (Fig. 3b). Estimates of the carbon content of *G. delicatula*, *P. alata*, *R. setigera* (Harrison et al. 2015) and *S. marinoi* (Norici et al. 2011) were applied at each station and vertically integrated by linear interpolation between the 3 depth levels (e.g. surface water, SCM and bottom water; Fig. 5) from the surface to the bottom of the euphotic zone. The carbon biomass of the most abundant species *G. delicatula* (268 pg C cell^{-1} and 0.059 pg C μm^{-3}; Harrison et al. 2015) accounted for 89% of the total biomass at the northernmost station (i.e. 1.9 gC m^{-2}) and decreased gradually to 26% at the southernmost station (Fig. 5a). *P. alata* accounted for 2–6% of the total biomass at the 2 southernmost stations (Fig. 5b), and contributions from the 2 other species accounted for less than 1% of the total biomass. Thus, the 4 species represented a majority of the total biomass in the northern part of the strait, whereas they only accounted for about a quarter of the phytoplankton biomass in the southern part. Uncertainties in these estimates may be due to variations in physiological characteristics (e.g. the influence of environmental conditions on the C-content). However, the gradual relative northward increase and estimated dominance of *G. delicatula* (i.e. from 0.47–1.9 g m^{-2}), and the corresponding decrease in *P. alata* (i.e. from 0.12 to < 0.01 g m^{-2}) and *R. setigera* (Fig. 3c), support the assumption that the variation of the 4 species is representative of a corresponding change in the phytoplankton community in the area.

An NMDS representation was obtained for the entire data set (stress = 0.04) based on the Bray-Curtis dissimilarity index of the log-transformed

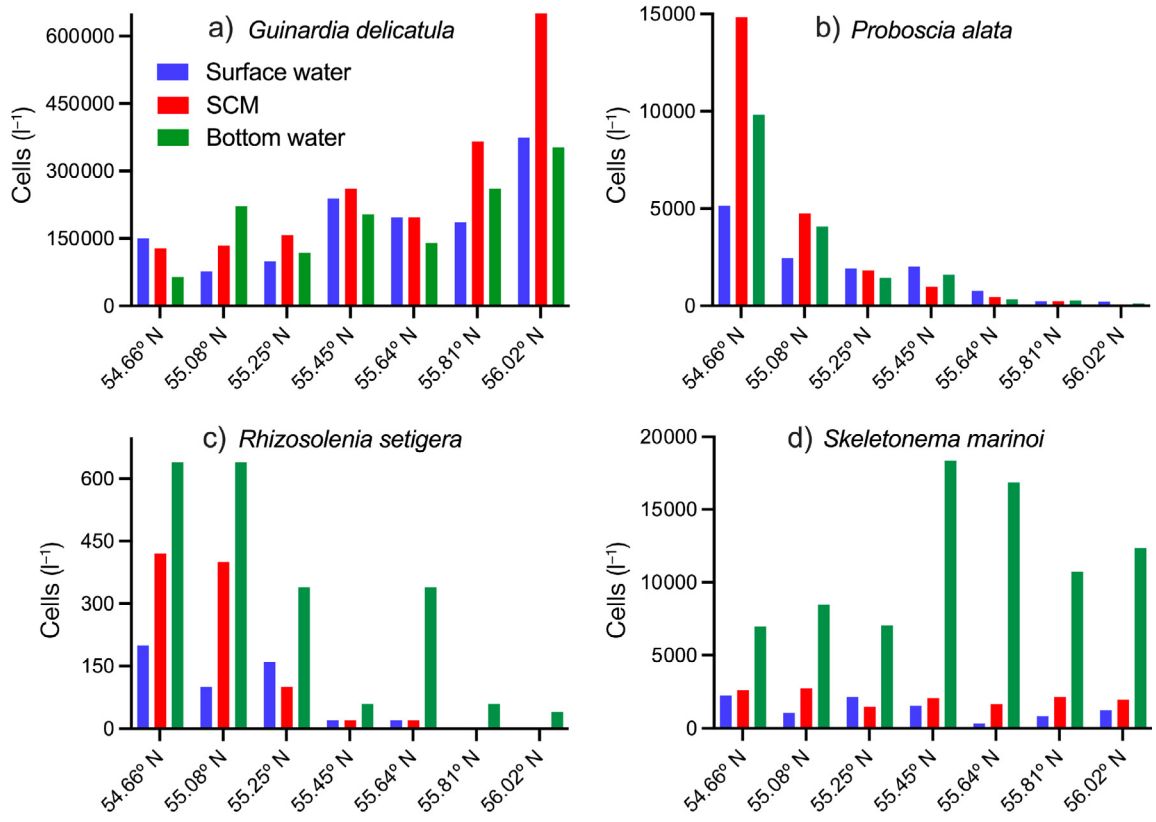

Fig. 5. Absolute cell counts of 4 diatom species: (a) *Guinardia delicatula*, (b) *Proboscia alata*, (c) *Rhizosolenia setigera*, and (d) *Skeletonema marinoi*. Values are shown for 7 stations along the strait (indicated by latitude) and at 3 depth levels: surface water (5 m); subsurface chloropyll maximum (SCM, mid-depth, 15 m) and bottom water (25 m). Note different scales

abundance of enumerated species (Fig. 6). The NMDS distribution was analyzed with respect to 2 groups representing surface samples (0–20 m) from the northern (Group A; >55.5° N) and southern part (Group B) of the strait and a group representing the bottom layer (Group C, ⩾20 m depth). An ANOSIM resulted in a significant grouping ($R = 0.59$, $p < 10^{-4}$) between the 3 compartments of the data set, thus supporting the conclusion that phytoplankton community compositions in the bottom and surface layers of the northern and southern parts of the strait were significantly different. The salinity of water samples with the bottom layer community decreased along the NMDS1-axis (not shown), and overlapping communities between the bottom water and surface water samples were found in the southern part of the strait (i.e. overlapping ellipses of the 95% confidence levels; Fig. 6). Overlapping confidence ellipses were also shown for the 2 surface groups, whereas the separated confidence intervals between the northern surface layer (Group A) and the bottom layer (Group C) showed a vertical separation of plankton communities at the northern entrance to the strait.

4. DISCUSSION

4.1. Overview

The relatively narrow Great Belt is a bottleneck of exchange between the North and Baltic Seas. Vertical mixing was significantly elevated in the strait and created a local habitat characterized by increased nutrient availability. We can estimate transport time for the surface water through the strait as well as the turbulent mixing of nutrients from the bottom and into the surface layer and assess changes in phytoplankton distributions and productivity against this background.

4.2. Vertical turbulent fluxes in the strait

The significance of the measured vertical turbulent fluxes and their impact on biological processes can be considered in relation to a time scale characterizing the flow through the strait. However, the 1 wk period over which we made our measurements was too short

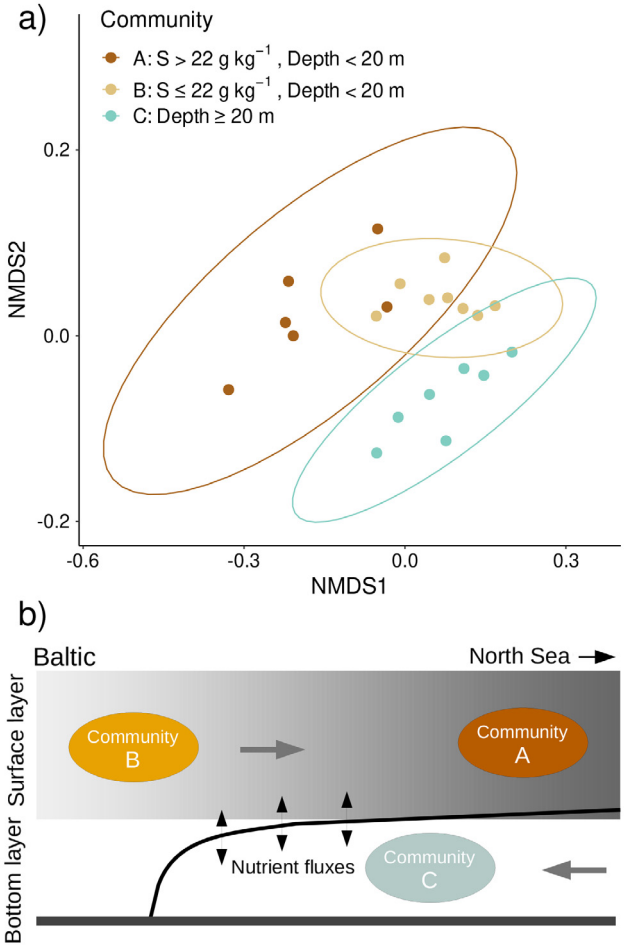

Fig. 6. (a) Non-metric multidimensional scaling (NMDS) plots of the 4 diatom species. Group A and B are low and high-saline surface samples, respectively, and bottom water is Group C (ellipses show 95% confidence of a bivariate normal distribution). (b) Conceptual figure of dominating transport patterns (gray arrows) and vertical mixing (black arrowheads) between the surface and bottom layer in the strait. Distinct communities (corresponding to Groups A–C) characterize the surface layers in the northern (Community A) and southern (Community B) parts of the strait and in the bottom layer (Community C)

to estimate the transport time. Therefore, a typical timescale for the transit through the strait was estimated by considering the average transport of water in the strait: a model-derived annual averaged surface layer (>15 m) outflow in the Great Belt of ~19 300 m^3 s^{-1} (Bendtsen et al. 2009) implies a mean flow of ~6.4 cm s^{-1} (using a width of ~20 km), and given the distance of 151 km between the 2 end-member stations, this corresponds to a transit time of 27 d. Similar analyses have been made for other periods, e.g. Hansen & Mohn (2021) found an average flow from the Baltic in the upper 14 m of ~16 200 m^3 s^{-1} for the period 2002–2019, corresponding to a transit time of 32 d. The estimated average speeds through the strait were also compared with ADCP measurements from 10 passages with an undulating ScanFish of a location in the center of the strait. The speed velocity along the strait was averaged in 5 min intervals in the upper 5 m and in the bottom layer (20–27 m depth) and ranged between 0.05 and 0.33 m s^{-1} with an average current speed (outflow is positive) in the surface layer (bottom layer) of 0.08 ± 0.15 m s^{-1} (−0.06 ± 0.15 m s^{-1}). These measurements were obtained at different times during a 4 d period and were, therefore, influenced by the tidal currents through the strait (the semidiurnal tidal range is less than 0.4 m). Thus, the current speed varies through the day due to both tides, wind, and surge effects. However, the relatively low current speeds show that the tidal excursion is less than ~15 km during a tidal period. Therefore, barotropic movement had a relatively small influence on the general transport in the surface and bottom layer through the strait.

On average, the passage through the strait takes ~30 d, and we apply this as a time scale for the flow. Vertical turbulent fluxes of salinity and nutrients are, therefore, assumed to modify surface concentrations along the strait during this relatively long period. Similarly, growth of phytoplankton, with typical cell division rates of about 1 d^{-1}, can maintain population integrity within the area and will have sufficient time to respond to a nutrient input during their passage through the strait.

The average salinity flux in the southern and northern sectors at 20 m of 9.6 × 10^{-3} g m^{-2} s^{-1} (Fig. 5c) implies a total flux of 25 kg m^{-2} from the bottom layer during the transit (30 d), corresponding to an average increase of S_A of 1.2 g kg^{-1} in the upper 20 m. The average change in S_A in the upper 20 m between the 2 sectors was 4.5 g kg^{-1} (i.e. corresponding to a salinity input of ~90 kg m^{-2} in the upper 20 m; Fig. 3a). Thus, the measured turbulent vertical mixing accounts for 27% of the observed salinity increase. This indicates that other mixing and exchange processes must also contribute to the observed salinity increase along the strait, e.g. localized mixing associated with reefs, shallow plateaus or other topographic constrictions that are not well captured in our data set.

4.3. NP and biological export

A noteworthy inverse relationship was seen between the distributions of NP and PP along the strait, i.e. NP was highest in the southern section of the strait while total PP was highest in the northern part

(Table 1). The significantly larger nitrate fluxes in the southern sector could explain the larger chlorophyll and PP in the northern sector by providing nutrients for growth of phytoplankton to the surface layer during the transit (Fig. 6b). The corresponding *F*-ratio (i.e. NP/PP) for the southern and northern sectors of 12 and 6%, respectively, also showed that the relative contribution of NP to PP was 2-fold greater in the southern than in the northern sector. The average NP in the 2 sectors of 0.054 g C m^{-2} d^{-1} corresponded to a NP of 1.6 g C m^{-2} when integrated over a period corresponding to the assumed transit time of 30 d. Thus, a significant amount of nitrate was supplied to the upper layer during the transit period. PP increased by about 0.09 g C m^{-2} d^{-1} from the southern to the northern sector, and this could easily be explained by NP.

From our data, we can estimate the potential contribution from NP that accumulates in the phytoplankton biomass (using chlorophyll concentration as a proxy for biomass). Vertically integrated chlorophyll increased significantly from 47 mg m^{-2} in the southern sector to 53 mg m^{-2} in the northern sector (Table 1). The northward chlorophyll increase corresponded to an increased biomass of 0.2 g C m^{-2} (C:chl ~ 40 g g^{-1}) during the transit. Considering that the vertical integral only includes the upper 20 m and that chlorophyll is relatively well mixed in the entire water column (Fig. 1c), this estimate of the biomass in the euphotic zone represents a minimum estimate and could be up to ~50% larger if the additional chlorophyll found between 20 m and the bottom of the euphotic zone is included. Thus, the northward increase in chlorophyll represents an increase of ~0.3 g C m^{-2} in biomass and this corresponds to only ~20% of NP. This suggests that the remaining ~80% may be returned to the bottom layer or other organic pools, e.g. via grazing or viral lysis, during the transit.

The gradual northward increase in nitrate deficit ($NO_3^\star$) in the surface layer (Fig. 1c) can potentially be explained by a gradual biological uptake during the transit. The potential for NP as an explanation for this horizontal increase in $NO_3^\star$ can be estimated from the accumulated NP during the transit (i.e. 1.6 g C m^{-2}) averaged in the euphotic zone and converted to nitrogen uptake via a molar C:N ratio (6.6). This results in a potential $NO_3^\star$ of 0.68 mmol m^{-3} in the northern part of the strait. The observed $NO_3^\star$ between the northern and southern sectors was 2.5 mmol m^{-3}. Thus, the estimated NP could only account for ~27% of the observed $NO_3^\star$. This implies that more nitrate had been available for biological consumption than was provided by the nutrient fluxes estimated here. This is in accordance with the conclusions from the salinity balance, i.e. that additional mixing in the strait similarly was required for explaining the salinity gradient along the strait.

4.4. Transport, mixing, and growth of phytoplankton

Groupings of phytoplankton inferred from the NMDS analysis can be interpreted in relation to the general circulation in the strait (Fig. 6). A clear separation of communities in the surface and bottom layers characterized the northern part of the strait. This separation is in accordance with the observed limited vertical mixing in the northernmost part of the strait ($K_v < 10^{-5}$ m^2 s^{-1}; Fig. S2). Thus, the slow vertical exchange would allow communities to evolve independently. Mixing between bottom and surface waters increased in the strait towards the south (Fig. 4c), and this might explain the overlapping communities between bottom and surface waters in the southern part of the strait (i.e. between Group B and C; Fig. 6).

Three of the 4 species, with *Skeletonema marinoi* being the exception, showed a gradual variation along the strait with either a maximum in the southern section (*Proboscia alata* and *Rhizosolenia setigera*) or northern section (*Guinardia delicatula*) of the strait. The gradual variation was also indicated in the NMDS representation where the southern section (Group B) exhibited only minor overlap with the northern section of the strait (Group A). This variation cannot be explained by the dominating transport pattern in the strait, e.g. the southern group would be expected to dominate through the entire strait if plankton distributions only were modified by advection. Similarly, the northward increase of *G. delicatula* cannot be explained solely by advection and none of the species are known to have a significant sensitivity to salinity in the salinity range observed in the strait. Thus, other processes influence the abundance of the 4 diatom species along the strait.

4.5. Light and nutrient limitation

The distribution of *G. delicatula* at the surface and the SCM increases gradually from ~150 000 cells l^{-1} at the southernmost station to 300 000–600 000 cells l^{-1} at the northern end of the strait, while *P. alata* and *R. setigera* almost completely disappear from initial concentrations of ~10^4 and ~10^2 cells l^{-1}, respectively

Table 2. Biovolume of the 4 centric diatoms enumerated from microscopy of preserved samples from the cruise. Estimates of biovolume assumed a cylinder form (volume = $d^2\,h\,\pi/4$), where d and h are diameter and height, respectively, except for *Skeletonema marinoi* where the volume was approximated from a cylinder with 2 half spheres, i.e. volume = $d^2\,\pi\,(h/4 + d/6)$ (Hillebrand et al. 1999)

Cell size	*Guinardia delicatula*	*Proboscia alata*	*Rhizosolenia setigera*	*Skeletonema marinoi*
h (µm)	32.4	442.7	417.1	7.2
d (µm)	9.4	6.7	24.8	4.6
Cell volume (µm^3)	2249	15608	201481	171

(Fig. 5). Comparison of cell volumes showed that *G. delicatula* was significantly smaller (~2200 µm^3; Table 2) than *P. alata* and *R. setigera* (~16 000 and ~200 000 µm^3, respectively). This suggests that biovolumes and associated traits may explain the different responses of these species to increased nutrient availability in the strait. Smaller cells tend to have a larger photosynthetic efficiency (Edwards et al. 2015, Richardson et al. 2016), where the photosynthetic response at low light levels (e.g. α^B) and P^B_{max} have been found to increase with decreasing cell size, possibly at the cost of a larger N-demand (Edwards et al. 2015). Thus, light limitation and nutrient-replete conditions in the strait would, in general, favor smaller cell sizes in accordance with the observed increase of *G. delicatula* and corresponding decrease in *P. alata* and *R. setigera* (i.e. *G. delicatula* is the smallest of these 3 relatively large diatoms). This could also explain the distribution of the small *S. marinoi* under the nutrient-rich and low light conditions in the bottom layer. Increasing bottom concentrations towards the south of *P. alata* and *R. setigera* could be explained by sinking of cells from the surface layer.

5. CONCLUSIONS

Vertical turbulent nitrate fluxes and the estimated NP of ~50 mg C m^{-2} d^{-1} were, on average, found to be 6–10 times larger in the strait than at stations located outside and at the entrances to the strait. Thus, we conclude that NP in the strait is at least an order of magnitude greater than observed at stations outside the strait area. Four dominating diatom species showed a significant grouping of communities between the surface in the northern and southern sections of the strait and between the surface and the bottom layer. The community distributions could not be explained by the general circulation in the strait. However, the gradual increase of the most abundant species (*Guinardia delicatula*) could easily be accounted for by the increased nutrient supply in the strait. We speculate that the gradual dominance of this species is associated with generally more efficient light usage for photosynthesis of small phytoplankton cells. This could also explain the presence of the small diatom *Skeletonema marinoi* in the bottom layer. Thus, low light and nutrient-replete conditions due to turbulent mixing appear to favor the growth of smaller cells during the passage of the strait and impact the community structure of phytoplankton in the transition zone between the Baltic Sea and the North Sea.

Acknowledgements. We thank the captain and crew of the RV 'Aurora' for helpful assistance during the cruise. This study was supported by the Danish National Science Foundation via its support of the Centre for Macroecology, Evolution, and Climate (grant no. DNRF96). The Velux Foundations (grant no. 00013281) provided support for the analysis of the measurements. The Carlsberg foundation provided support for the turbulence instrument (CF15-0301). The Cids-2 cruise was also supported by the Danish Centre for Marine Research (2018-05). Satellite-derived PAR was obtained from the NASA Goddard Space Flight Center, Ocean Ecology Laboratory, Ocean Biology Processing Group (2014) MODIS-Aqua Ocean Color Data.

LITERATURE CITED

Arnholt AT, Evans B (2021) BSDA: basic statistics and data analysis. R package version 1.2.1. https://CRAN.R-project.org/package=BSDA

Bendtsen J, Richardson K (2018) Turbulence measurements suggest high rates of new production over the shelf edge in the north-eastern North Sea during summer. Biogeosciences 15:7315–7332

Bendtsen J, Gustafsson KE, Söderkvist J, Hansen JLS (2009) Ventilation of bottom water in the North Sea — Baltic Sea transition zone. J Mar Syst 75:138–149

Bouffard D, Boegman L (2013) A diapycnal diffusivity model for stratified environmental flows. Dyn Atmos Oceans 61–62:14–34

Douglas W, Lueck R (2015) ODAS MATLAB Library, technical manual version 4.0. Rockland Scientific International, Victoria

Dugdale RC, Goering JJ (1967) Uptake of new and regenerated forms of nitrogen in primary productivity. Limnol Oceanogr 12:196–206

Edwards KF, Thomas MK, Klausmeier CA, Litchman E (2015) Light and growth in marine phytoplankton: allometric, taxonomic and environmental variation. Limnol Oceanogr 60:540–552

Frouin R, McPherson J, Ueyoshi K, Franz BA (2012) A time series of photosynthetically available radiation at the ocean surface from SeaWiFS and MODIS data. Proc SPIE 8525:852519

GEBCO Bathymetric Compilation Group (2020) The GEBCO_2020 Grid—a continuous terrain model of the global oceans and land. British Oceanographic Data Centre, National Oceanography Centre, NERC, Liverpool

Grasshoff K, Ehrhardt M, Kremling K (1983) Methods of seawater analysis, 2nd edn. Verlag Chemie, Weinheim

Hansen JLS, Bendtsen J (2013) Parameterisation of oxygen dynamics in the bottom water of the Baltic Sea–North Sea transition zone. Mar Ecol Prog Ser 481:25–39

Hansen JLS, Bendtsen J (2014) Seasonal bottom water respiration in the North Sea–Baltic Sea transition zone: rates, temperature sensitivity and sources of organic material. Mar Ecol Prog Ser 499:19–34

Hansen JLS, Mohn C (2021) Hydrografi. In: Hansen JW, Høgslund S (eds) Marine områder 2019. NOVANA. DCE –Danish Centre for Environment and Energy, Aarhus University, p 24–40

Harrison PJ, Zingone A, Mickelson MJ, Lehtinen S and others (2015) Cell volumes of marine phytoplankton from globally distributed coastal data sets. Estuar Coast Shelf Sci 162:130–142

HELCOM (2021) Guidelines for monitoring of phytoplankton species composition, abundance and biomass. http://dx.doi.org/10.25607/OBP-1822

Henriksen P (2009) Long-term changes in phytoplankton in the Kattegat, the Belt Sea, the Sound and the western Baltic Sea. J Sea Res 61:114–123

Herlemann DPR, Labrenz M, Jürgens K, Bertilsson S, Waniek JJ, Andersson AF (2011) Transitions in bacterial communities along the 2000 km salinity gradient of the Baltic Sea. ISME J 5:1571–1579

Hillebrand H, Dürselen CD, Kirschtel D, Pollingher U, Zohary T (1999) Biovolume calculation for pelagic and benthic microalgae. J Phycol 35:403–424

IOC, SCOR, IAPSO (2010) The international thermodynamic equation of seawater–2010: calculation and use of thermodynamic properties. Manuals and Guides No. 56, Intergovernmental Oceanographic Commission, UNESCO

Jakobsen F, Trébuchet C (2000) Observations of the transport through the belt sea and an investigation of the momentum balance. Cont Shelf Res 20:293–311

Jakobsen HH, Markager S (2016) Carbon-to-chlorophyll ratio for phytoplankton in temperate coastal waters: seasonal patterns and relationship to nutrients. Limnol Oceanogr 61:1853–1868

Lehmann A, Myrberg K, Post P, Chubarenko I and others (2022) Salinity dynamics of the Baltic Sea. Earth Syst Dyn 13:373–392

Lueck R (2016) Calculating the rate of dissipation of turbulent kinetic energy (RSI Technical Note 028). Rockland Scientific International, Victoria

Lund-Hansen LC, Nielsen MH, Bruhn A, Christiansen C, Vang T, Richardson K, Ayala P (2008) A consistent high primary production and chlorophyll-a maximum in a narrow strait — effects of hydraulic control. J Mar Syst 74:395–405

Lyngsgaard MM, Richardson K, Markager S, Nielsen MH, Olesen M, Christensen JP (2014) Deep primary production in coastal pelagic systems: importance for ecosystem functioning. Mar Ecol Prog Ser 517:15–33

Norici A, Bazzoni AM, Pugnetti A, Raven JA, Giordano M (2011) Impact of iradiance on the C allocation in the coastal marine diatom *Skeletonema marinoi* Sarno & Zingone. Plant Cell Environ 34:1666–1677

Oksanen JF, Blanchet G, Friendly M, Kindt R and others (2020) Vegan: community ecology package. R package version 2.5-7. https://CRAN.R-project.org/package=vegan

Osborn TR (1980) Estimate of the local rate of vertical diffusion from dissipation measurements. J Phys Oceanogr 10: 83–89

R Core Team (2021) R: a language and environment for statistical computing. R Foundation for Statistical Computing, Vienna

Redfield AC, Ketchum BH, Richards FA (1963) The influence of organisms on the composition of sea water. In: Hill MN (ed) The sea. Wiley-Interscience, New York, NY, p 26–77

Reissmann JH, Burchard H, Hagen RFE, Lass HU, Nausch VMG, Umlauf L, Wieczorek G (2009) Vertical mixing in the Baltic Sea and consequences for eutrophication — a review. Prog Oceanogr 82:47–80

Richardson K, Bendtsen J, Kragh T, Mousing EA (2016) Constraining the distribution of photosynthetic parameters in the global ocean. Front Mar Sci 3:269

Rydberg L, Ærtebjerg G, Edler L (2006) Fifty years of primary production measurements in the Baltic entrance region, trends and variability in relation to land-based input of nutrients. J Sea Res 56:1–16

Stanev EV, Pein J, Grashorn S, Zhang YJ, Schrum C (2018) Dynamics of the Baltic Sea Straits via numerical simulation of exchange flows. Ocean Model 131:40–58

Utermöhl H (1958) Zur Vervollkommnung der quantitativen Phytoplankton-Methodik. Mitt Int Ver Theor Angew Limnol 9:1–38

Wasmund N, Tuimala J, Suikkanen S, Vadepitte L, Kraberg A (2011) Long-term trends in phytoplankton composition in the western and central Baltic Sea. J Mar Syst 87:145–159

Webb WL, Newton M, Starr D (1974) Carbon dioxide exchange of *Alnus rubra*. A mathematical model. Oecologia 17:281–291

Wolk F, Yamazaki H, Seuront L, Lueck RG (2002) A new free-fall profiler for measuring bio-physical microstructure. J Atmos Ocean Technol 19:780–793

Editorial responsibility: Just Cebrian, San Francisco, California, USA
Reviewed by: 3 anonymous referees

Submitted: April 13, 2023
Accepted: November 13, 2023
Proofs received from author(s): January 21, 2024